INSTITUTE OF PLASMA PHYSICS

NAGOYA UNIVERSITY

ALPHA-PARTICLE SIMULATION
USING NBI BEAM AND ICRF WAVE

Y. Ogawa and Y. Hamada

(Received June 1, 1984)

IPPJ-688 July 1984

RESEARCH REPORT

NAGOYA, JAPAN

ALPHA-PARTICLE SIMULATION USING NBI BEAM AND ICRF WAVE

Y. Ogawa and Y. Hamada

(Received - June 1, 1984)

IPPJ - 688 July 1984

Further communication about this report is to be sent to the Research Information Center, Institute of Plasma Physics, Nagoya University, Nagoya 464, Japan.

Abstract

A new idea to produce the distribution function similar to that of alpha-particles in an ignited plasma has been proposed. This concept is attributed to the acceleration of the injected beam up to about 1 MeV/nucleon by the ICRF wave with cyclotron higher harmonics. This new method makes it possible to perform the simulation experiments for alpha-particles under the condition of moderate plasma parameters (e.g., T_e = 4 keV, n_e = 3.5×10^{19} m^{-3} and B_T = 3 T). And it is found that $3\omega_{ci}$ ICRF wave is preferable compared with other cyclotron harmonics, from the viewpoints of the effective tail formation with smaller bulk ion heating and lower amplitude of the applied electric field. The formula for the maximum energy of the extended beam is also derived.

(i) Introduction

Alpha-particles produced by DT reactions play an important role in an ignited plasma to sustain the bulk plasma temperature. To study behaviors of alpha-particles, experiments with a DT reacting plasma are necessary, but the number of DT discharges will be severely restricted because of the activation of the device by 14-MeV neutrons due to DT reactions. It has, therefore, a great advantage to simulate the behaviors of alpha-particles without using DT reacting plasmas. Some ideas to produce the distribution function similar to that of alpha-particles have been proposed by D. Post[1] and A. Iiyoshi[2], where ICRF (Ion Cyclotron Range of Frequency) wave has been applied for D-^{3}He plasma. The basic concept of these ideas is attributed to the acceleration of the Maxwellian-like tail of ^{3}He minority ions up to about 1 MeV/nucleon by the ICRF wave[3], but the experimental parameters for this method should be very restricted within the range of relatively high plasma temperature, low plasma density and high toroidal field (e.g., T_e = 10 keV, n_e = 2x10^{19} m^{-3} and B_T = 5 T in TFTR device)[1].

In this paper a new idea to produce the distribution function of the alpha-particles is proposed, where the injected beam is directly accelerated up to about 1 MeV/nucleon by the ICRF wave with cyclotron higher harmonics. It is expected that the energetic ions will couple more effectively with the ICRF wave of cyclotron higher harmonics. The distribution function of the injected beam has been calculated with a two-dimensional(2-D) linear Fokker-Planck code including the quasi-linear diffusion term due to the ICRF wave. The maximum

beam energy extended by the ICRF wave has been examined, and the formula for it has been also derived.

(ii) Basic equations and its computer code

The Fokker-Planck equation for the injected beam is given by

$$\frac{\partial}{\partial t} f_b(\vec{v}, t) = \frac{\partial f_b}{\partial t}\Big)_{coll.} + \frac{\partial}{\partial \vec{v}} \vec{D} \frac{\partial f_b}{\partial \vec{v}} + S_b \qquad (1)$$

where the first and second terms of the right-hand side denote the Coulomb collision only with bulk Maxwellian plasmas (ions and electrons) and the quasi-linear diffusion, respectively, and the last one is the source of the injected beam. The Coulomb collision term is given by ref.(4) in detail, and the quasi-linear diffusion term is written down as follows[3,5,6] ;

$$\frac{\partial}{\partial \vec{v}} \vec{D} \frac{\partial f_b}{\partial \vec{v}} = \frac{2Z_b^2 e^2}{m_b^2} \sum_k \sum_{n=-\infty}^{\infty} \hat{L} \frac{|\omega_{ci}^0|}{|n|\omega'^2_{ci}} \frac{\sqrt{\xi_2 - \xi_0} - \sqrt{\xi' - \xi_0}}{\xi_2 - \xi_1}$$

$$|\theta_{n,k}|^2 v_\perp^2 \hat{L} f_b(v_\perp, v_\parallel) \qquad (2)$$

where

$$\hat{L} \equiv \left(1 - \frac{k_\parallel v_\parallel}{\omega}\right) \frac{1}{v_\perp} \frac{\partial}{\partial v_\perp} + \frac{k_\parallel}{\omega} \frac{\partial}{\partial v_\parallel} \qquad (3)$$

$$|\theta_{n,k}|^2 = \frac{1}{8} E_R^2 J_{n+1}^2(b) + \frac{1}{8} E_L^2 J_{n-1}^2(b) + \frac{1}{2} \left(\frac{v_\parallel}{v_\perp}\right)^2 E_\parallel^2 J_n^2(b) \qquad (4)$$

$$\omega_{ci}' = (\omega - k_\parallel v_\parallel) / n$$

ω_{ci}^0 : cyclotron frequency at $R = R_0$

$$\xi_0 = (1 - \omega_{ci}^0/\omega_{ci}')^2 \qquad (5)$$

$$\xi_1 = (a_1/R_0)^2 \qquad \xi_2 = (a_2/R_0)^2$$

$$\xi' = \max (\xi_1, \xi_0)$$

$$b = k_\perp v_\perp / \omega'_{ci}$$

and

$$E_R = E_x - iE_y, \qquad E_L = E_x + iE_y \qquad (6)$$

The above equation has been derived after averaging the quasi-linear diffusion coefficient on the magnetic surface between the minor radii a_1 and a_2[5], as shown in Fig. 1. The major radius of the plasma is denoted by R_0, and the mass and charge number of the injected beam are m_b and Z_b, respectively. Three components of the electric field E_L, E_R and $E_\parallel$ denote the left- and right-hand polarized ones and the parallel one, respectively, but the parallel electric field $E_\parallel$ is neglected in the following calculations because of its relative smallness. The frequency of the applied ICRF wave is denoted by ω, and $k_\parallel$ and $k_\perp$ are parallel and perpendicular wave numbers, respectively, and $J_n(b)$ is the n-th Bessel function.

The dispersion relation of the fast wave has been solved for the cold plasma in order to determine the perpendicular wave number and the ratio of E_L to E_R. The amplitude of the electric field itself has been determined from the power absorption rate of the ICRF wave calculated by the following equation;

$$P_{abs} = \int \frac{1}{2} m v^2 \frac{\partial}{\partial \vec{v}} (\vec{D} \frac{\partial f_b}{\partial \vec{v}}) \cdot d\vec{v} \qquad (7)$$

In the computer code, 2-D velocity space is divided by (v,θ) mesh, where v is a velocity and θ is a pitch angle. The minimum energy E_{min} is chosen to be $2T_i$. To verify the computer code concerning to the quasi-linear diffusion term, the power absorption rates for the Maxwellian ion distribution function have been evaluated for the cases of $2\omega_{ci}$ and $3\omega_{ci}$ cyclotron harmonics. By using the quasi-linear diffusion term given by eq. (2), the power absorption rates in the cases of $\omega = 2\omega_{ci}^0$ and $3\omega_{ci}^0$ are derived as follows:

$$P_{abs}^{II} \simeq \frac{R_0}{a}\left(\frac{k_\perp v_{th,i}}{\omega_{ci}^0}\right)^2\left(\frac{c}{v_A}\right)^2\cdot\frac{1}{8}\cdot\left(\frac{\varepsilon_0|E_L|^2}{2}\right)\cdot\omega_{ci}^0 \qquad (8)$$

$$P_{abs}^{III} \simeq \frac{R_0}{a}\left(\frac{k_\perp v_{th,i}}{\omega_{ci}^0}\right)^4\left(\frac{c}{v_A}\right)^2\cdot\frac{1}{64}\cdot\left(\frac{\varepsilon_0|E_L|^2}{2}\right)\cdot\omega_{ci}^0 \qquad (9)$$

where a ($(a_1+a_2)/2$) is a minor radius, $v_{th,i}$ is the thermal velocity of the ion ($v_{th,i}^2 = 2T_i/m_i$), and c and v_A are the light and Alfven velocities, respectively. Here the power absorption rate due to E_R field is neglected, because it becomes very small by a factor of $(k_\perp v_{th,i}/\omega_{ci})^4 << 1$, compared with that due to E_L field.

The power absorption rates in the cases of $2\omega_{ci}$ and $3\omega_{ci}$ have been also calculated with the computer code for the Maxwellian ion distribution function, and found to be consistent with those evaluated by eqs. (8) and (9) within about 10 % accuracy.

(iii) High-energy tail formation of 120-keV D-beam due to $3\omega_{ci}$ ICRF wave

Calculations have been performed by using parameters of R-tokamak[7] ; that is, the major R_0 and minor a_0 radii of the plasma are 2.09 m and 0.76 m, respectively, the toroidal field B_T is 3 T, and the plasma current I_P is 3 MA. The minor radius of the calculational magnetic surface is chosen to be $(a_1 + a_2)/2 = 0.3 \cdot a_0$. The parameters of the bulk plasma assumed in the Fokker-Planck calculations are as follows; T_e = 4 keV, T_i = 5 keV, n_e = 3.5×10^{19} m^{-3}, Z_{eff} = 1 and the mass number of bulk ion is 2.5. A 120-keV D-beam of 15 MW is injected into the plasma, which gives the input power density of 0.6 w/cm^3. This input power is, eventually, consumed by the bulk plasma heating, since the loss cone in the velocity space is not taken into account. The parallel wave number of the applied ICRF wave is assumed to be 3.3 m^{-1}.

Figure 2 shows the contour of the deuterium distribution function in $(v_\parallel, v_\perp)$ space, in the case that $3\omega_{ci}$ ICRF wave has been imposed on the injected D-beam. The high-energy tail much larger than the initial beam energy(120 keV) has been produced toward the perpendicular direction. Then, the relatively anisotropic distribution function has been formed, because the pitch angle scattering due to the bulk ions decreases as the energy of tailed D-beam increases.

The time evolution of the distribution function for the injected D-beam is given in Fig. 3, after integrating the 2-D distribution function with respect to the pitch angle. At 1.2 sec the beam energy extends up to 1.8 MeV, which corresponds to

the velocity of alpha-particles (3.5 MeV) produced by DT reactions. Another remarkable point is that the distribution function does not run away, but becomes steady state after a few seconds, because, as the energy increases, the Coulomb drag due to bulk electrons is enhanced and the power input of the ICRF wave to the high energy ions reaches the maximum value in accordance with the characteristics of the Bessel function in eq.(4). Here, we should notice that the argument of the Bessel function becomes greater than unity at $E_b > 60$ keV for $3\omega_{ci}$ ICRF wave.

The time evolutions of the beam density, the total beam energy and the power absorption rate due to the ICRF wave are shown in Fig. 4, where 15-MW D-beam is continuously injected and $3\omega_{ci}$ ICRF wave is switched on at 0.4 sec. According to the growth of the high-energy tail by applying the ICRF wave, the moderate increase of the beam density and the strong enhancement of the power absorption rate can be seen. The power absorption rate is about 0.2 w/cm^3 just after the onset of the ICRF wave, and increases up to about 1 w/cm^3 after a few seconds. Since the increase of the beam density is not so large, it is considered that the ICRF power is selectively absorpted in the extended high-energy tail, because of the large Larmor radius comparable or larger than the perpendicular wave length. It has been also reported in the present experiments of $2\omega_{ci}$ heating[8] that the quasi-linear damping is much stronger than the linear damping, because of the formation of the high energy tail.

In Fig. 5, the steady-state distribution functions are shown for different power absorption rates, where the amplitudes

of the applied E_R field are 4.67, 6.44, 7.05 and 7.61 kV/m for P_{abs} = 0.1, 0.43, 0.72 and 1.09 w/cm^3, respectively. The power absorption rate is roughly proportional to 4th - 5th power of the applied electric field strength. When the absorption power becomes greater than 0.4 w/cm^3, the beam tail can be extended up to 1.8 MeV, and the amount of this high energy tail is roughly proportional to the absorpted power.

(iv) Comparison of the high-energy tail formations by the ICRF wave for various cyclotron harmonics

In the previous discussion, it is shown that $3\omega_{ci}$ ICRF wave is applicable to extend 120-keV D-beam up to the velocity of 3.5-MeV alpha particles. Here, the possibility of the high energy tail production with other cyclotron harmonics has been examined. In Fig. 6, the steady-state distribution functions are presented in the cases of $2\omega_{ci}$, $3\omega_{ci}$ and $4\omega_{ci}$ ICRF waves, comparing that of alpha-particles corresponding to the fusion output of 200 MW. For these cyclotron harmonics Table I summarizes the perpendicular wave number $k_\perp$, the ratio of E_L field to E_R one calculated with the dispersion relation, the amplitude of E_R electric field itself, and the power rates absorpted by the Maxwellian bulk ions and the injected D beam. The power absorption rates in the velocity space are shown in Fig. 7 in the cases of $2\omega_{ci}$ and $3\omega_{ci}$ ICRF waves, where the value of Y-axis is the power absorption rate integrated from the minimum energy (E_{min} = 10 keV) to the beam energy (E_b).

In the case of $2\omega_{ci}$ ICRF wave, 40% of the total wave power is consumed by the bulk ion heating. From the viewpoint of the

effective high-energy tail formation with smaller ICRF wave power, the direct heating of the bulk ions by the applied ICRF wave is not preferable. In addition, the large fraction of the power absorpted by the D-beam deposites in the relatively lower energy range (E_b < 0.6 MeV), as shown in Fig. 7(a). Accordingly, the high-energy particles larger than 1.2 MeV can not be produced effectively. Therefore, $2\omega_{ci}$ ICRF wave seems to be inapplicable for the high-energy tail formation up to the alpha-particle's velocity.

In the case of $3\omega_{ci}$ ICRF wave, the power absorpted by the bulk ions is negligibly small compared with that by the D-beam, and the ICRF wave power deposites up to the energy range of 1.8 MeV in the velocity space. It is, then, confirmed in Fig. 6 that the D-beam distribution function is extended up to 1.8 MeV by $3\omega_{ci}$ ICRF wave, and becomes similar to that of the alpha-particles for 200-MW fusion output. Therefore, it seems that $3\omega_{ci}$ ICRF wave is applicable for this simulation experiment.

When $4\omega_{ci}$ ICRF wave is applied, the distribution function similar to that of the alpha-particles can be also produced, as shown in Fig. 6, because $4\omega_{ci}$ ICRF wave couples strongly with higher energy ions. But we should notice that the applied electric field becomes very large (E > 10 kV/m). Then, this might restrict the usage of $4\omega_{ci}$ ICRF wave for this study.

(v) Discussion for the maximum energy of the extended beam

With moderate plasma parameters(e.g., T_e = 4 keV, n_e = 3.5×10^{19} m^{-3} and B_T = 3 T), the injected beam is gradually

extended up to 1.8 MeV or more by $3\omega_{ci}$ ICRF wave. This extension, however, does not occur, when the toroidal field is reduced from 3 T to 2 T, or when the bulk plasma density is increased from 3.5×10^{19} m^{-3} to 7.0×10^{19} m^{-3}. Figure 8 shows the distribution functions for a) a lower toroidal field case (B_T = 2 T) and b) a higher density one (n_e = 7.0×10^{19} m^{-3}), comparing with c) the standard one (B_T = 3 T and n_e = 3.5×10^{19} m^{-3}). The distribution functions in the cases of lower B_T and higher n_e decrease abruptly at the beam energy of 1.5 MeV and 1.6 MeV, respectively. The maximum energy of this extended beam may be explained by the characteristics of the Bessel function included in the quasi linear diffusion coefficient.

The Bessel function itself is plotted in Fig. 9(a), and the term $|\theta_{n,k}|^2$ in the quasi-linear diffusion coefficient, defined by eq. (4), is also plotted for $2\omega_{ci}$, $3\omega_{ci}$ and $4\omega_{ci}$ ICRF waves in Fig. 9(b). When the ion energy is so small that the argument of the Bessel function is less than unity, the term $|\theta_{n,k}|^2$ increases according to (n-1)-th Bessel function stems from the left-hand polarized electric field. Then the term $|\theta_{n,k}|^2$ reaches the peak and begins to decrease to the minimum point, which is roughly corresponding to the zero-point of (n+1)-th Bessel function comes from the right-hand one, because the right-hand polarized electric field is much larger than the left-hand one. Taking into account the increase of the Coulomb drag due to bulk electrons according to the increase of the beam energy, it is expected that the extension of the beam energy stops at the energy corresponding to the minimum value of the term $|\theta_{n,k}|^2$ at most. This is why the distribution function

does not run away and becomes steady state.

The above consideration is supported by the the results shown in Fig. 8, because the first zero-point of 4-th Bessel function in the case of $3\omega_{ci}$ ICRF wave is 7.59 and corresponding energies for this argument are 1.57 MeV, 1.74 MeV and 3.53 MeV for these three cases (a) B_T = 2 T, b) n_e = 7.0×10^{19} m^{-3} and c) standard case), respectively.

Then we say that by using the argument of the Bessel function the maximum energy of the extended beam can be expressed as follows;

$$E_{max} \sim \frac{1}{2}m_b\left(\frac{\omega_{cb}}{k_\perp}b_{n+1}\right)^2 \qquad (10)$$

where b_{n+1} is the argument of the first zero-point of (n+1)-th Bessel function. This formula suggests that the experiment with higher toroidal field and/or the lower plasma density is appropriate to produce a high-energy beam.

(v) Summary

In conclusion, it is shown that 120-keV D-beam is extended up to the velocity of 3.5-MeV alpha-particles by applying ICRF wave with cyclotron higher harmonics, and the similar distribution function of alpha-particles in an ignited DT plasma can be produced effectively. This new method makes it possible to perform the simulation experiment with moderate plasma parameters (relatively lower plasma temperature, higher plasma density and lower toroidal field), e.g., T_e = 4 keV, n_e = 3.5×10^{19} m^{-3} B_T = 3 T. Some physical problems related to

alpha-particles may be examined by using this extended distribution function, although the beam distribution function is very anisotropic toward the perpendicular direction, and it is not possible to produce the inversion of the distribution function which occurs at the initial stage of DT burning plasma. It is found that the injected beam accelerated by the ICRF wave does not run away, but stops at the energy corresponding to the first zero-point of (n+1)-th Bessel function included in the quasi-linear diffusion coefficient. And the formula for the maximum energy of the extended beam is also derived. In comparison with various cyclotron harmonics of the ICRF wave from the viewpoints of the effective beam tail formation with a smaller bulk ion heating and a lower amplitude of the RF field, it is concluded that $3\omega_{ci}$ ICRF wave will be most applicable for the simulation experiment of alpha-particles.

Acknowlegdements

The authors would like to thank Dr. T. Watari and Dr. T. Amano for fruitful discussions.

References

(1) D. Post et al., J. Vac. Sci. Technol.A, 1 (1983) 206

(2) A. Iiyoshi, private communication

(3) T.H. Stix, Nucl. Fusion, 15 (1975) 737

(4) R.H. Fowler et al., ORNL/TM-5487, (July, 1976)

(5) M. Mori, Univ. of Tokyo, Ph. D. thesis (May, 1981)

(6) C.F. Kennel and F. Engelmann, Phys. Fluid, 9 (1966) 2377

(7) Y. Abe et al., "DT Burning Tokamak with Low-Activation Materials --Reacting Plasma Project--", presented at 10th Symp. on Fusion Engineering, Philadelphia, USA, Dec. 5-9, 1983

(8) D.Q. Hwang et al., Phys. Rev. Lett., 51 (1983) 1865

Table and Figure Captions

Table. 1. The perpendicular wave number $k_\perp$, the ratio of the left-hand polarized electric field (E_L) to the right-hand one (E_R), the amplitude of E_R field itself and the power rates absorpted by the bulk ions (P_{bulk}) and the injected D-beam (P_{beam}) for $2\omega_{ci}$, $3\omega_{ci}$ and $4\omega_{ci}$ ICRF waves.

Fig. 1. Toroidal geometry The cyclotron resonance layer locates at the position of $\omega = n\omega_{ci}$. The quasi-linear diffusion coefficient has been averaged on the magnetic surface between the minor radii a_1 and a_2.

Fig. 2. Contour of the steady-state distribution function for the D-beam, when $3\omega_{ci}$ ICRF wave is applied. 120-keV D-beam is continuously injected at the pitch angle of 60°, and the power absorption rate of $3\omega_{ci}$ ICRF wave is 1.09 w/cm^3.

Fig. 3. Time evolution of the 1-D distribution function of the D-beam integrated with respect to the pitch angle, when $3\omega_{ci}$ ICRF wave has been applied.

Fig. 4. Time evolutions of the beam density, the total beam energy and the power absorption rate. The power density of 120-keV D-beam is 0.6 w/cm^3, and $3\omega_{ci}$ ICRF wave has been switched on at 0.4 sec.

Fig. 5. The steady-state distribution functions for

different power absorption rates. The amplitudes of the applied E_R field are 4.67, 6.44, 7.05 and 7.61 kV/m for P_{abs} = 0.1, 0.43, 0.72 and 1.09 w/cm^3, respectively.

Fig. 6. The steady-state distribution functions of the extended D-beam in the cases of $2\omega_{ci}$, $3\omega_{ci}$ and $4\omega_{ci}$ ICRF waves, and that of alpha-particles for the fusion output of 200 MW. The energy axis (x-axis) is assigned by the same particle velocity. The perpendicular wave number and the applied electric field strength are summarized in Table 1.

Fig. 7. The power absorption rate in the velocity space in the cases of $2\omega_{ci}$ and $3\omega_{ci}$ ICRF waves. Y-axis denotes the power absorption rate integrated from the minimum energy (E_{min} = 10 keV) to the beam energy (E_b).

Fig. 8. The steady-state distribution function in the cases of a) the lower toroidal field (B_T = 2 T), b) the higher plasma density (n_e = 7.0x10^{19} m^{-3}) and c) the standard parameters (B_T = 3 T and n_e = 3.5x10^{19} m^{-3}), when $3\omega_{ci}$ ICRF wave has been applied. The energies corresponding to the first zero-point of 4-th Bessel function are a) 1.57 MeV, b) 1.74 MeV and c) 3.53 MeV for these three cases, respectively, and the two former are shown in this figure.

Fig. 9. a) Square of n-th Bessel function ($J_n^2(b)$) as a function of the argument, and b) the value $|\hat{\theta}_{n,k}|^2$ defined as $J_{n+1}^2(b) + (E_L/E_R)^2 * J_{n-1}^2(b)$, extracted from the quasi-linear diffusion coefficient $|\theta_{n,k}|^2$,

neglecting $E_{\parallel}$ term. The ratios of E_L to E_R are 0.393, 0.554 and 0.649 for $2\omega_{ci}$, $3\omega_{ci}$ and $4\omega_{ci}$, respectively.

Table 1

	$2\omega_{ci}$	$3\omega_{ci}$	$4\omega_{ci}$
Perpendicular wave number ($k_\perp$: 1/m)	39.3	59.3	79.5
E_L/E_R	0.393	0.554	0.649
Amplitude of E_R (kV/m)	4.76	7.61	11.63
Bulk ions (P_{bulk}: w/cm^3)	0.375	0.0245	0.0022
D-beam (P_{beam}: w/cm^3)	0.610	1.09	1.04

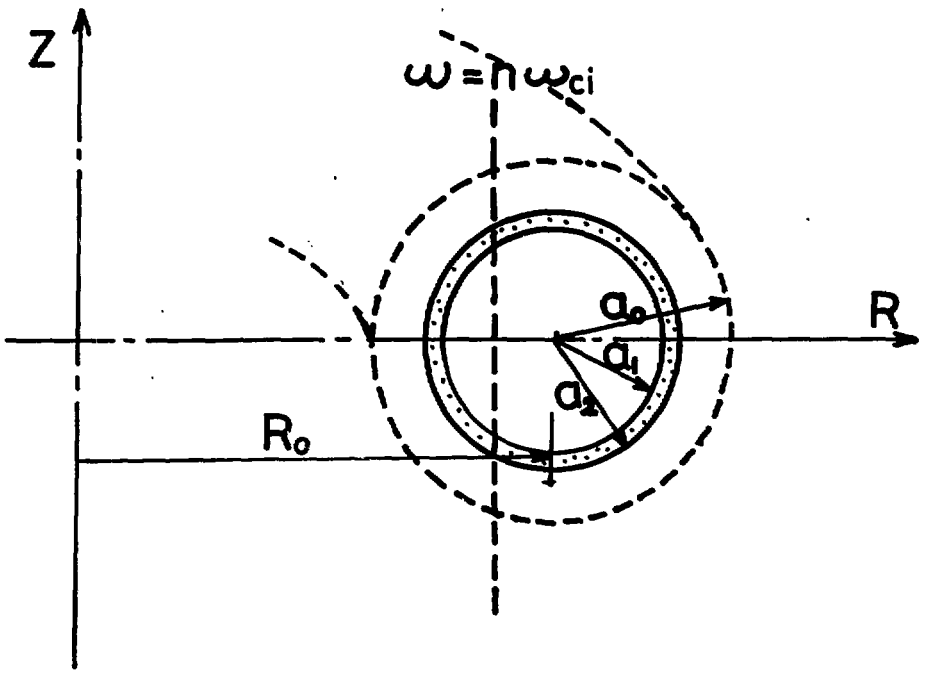

Fig. 1

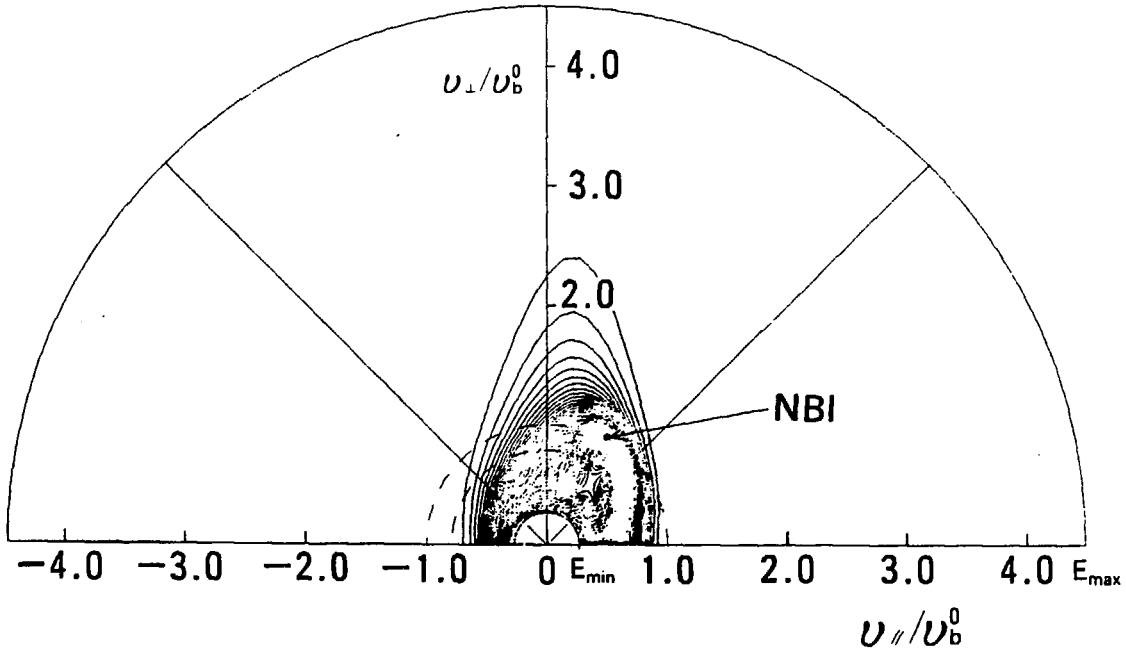
$\upsilon_\perp/\upsilon_b^0$
4.0
3.0
2.0
NBI
−4.0
−3.0
−2.0
−1.0
0
E_{min}
1.0
2.0
3.0
4.0
E_{max}
$\upsilon_{//}/\upsilon_b^0$

Fig. 2

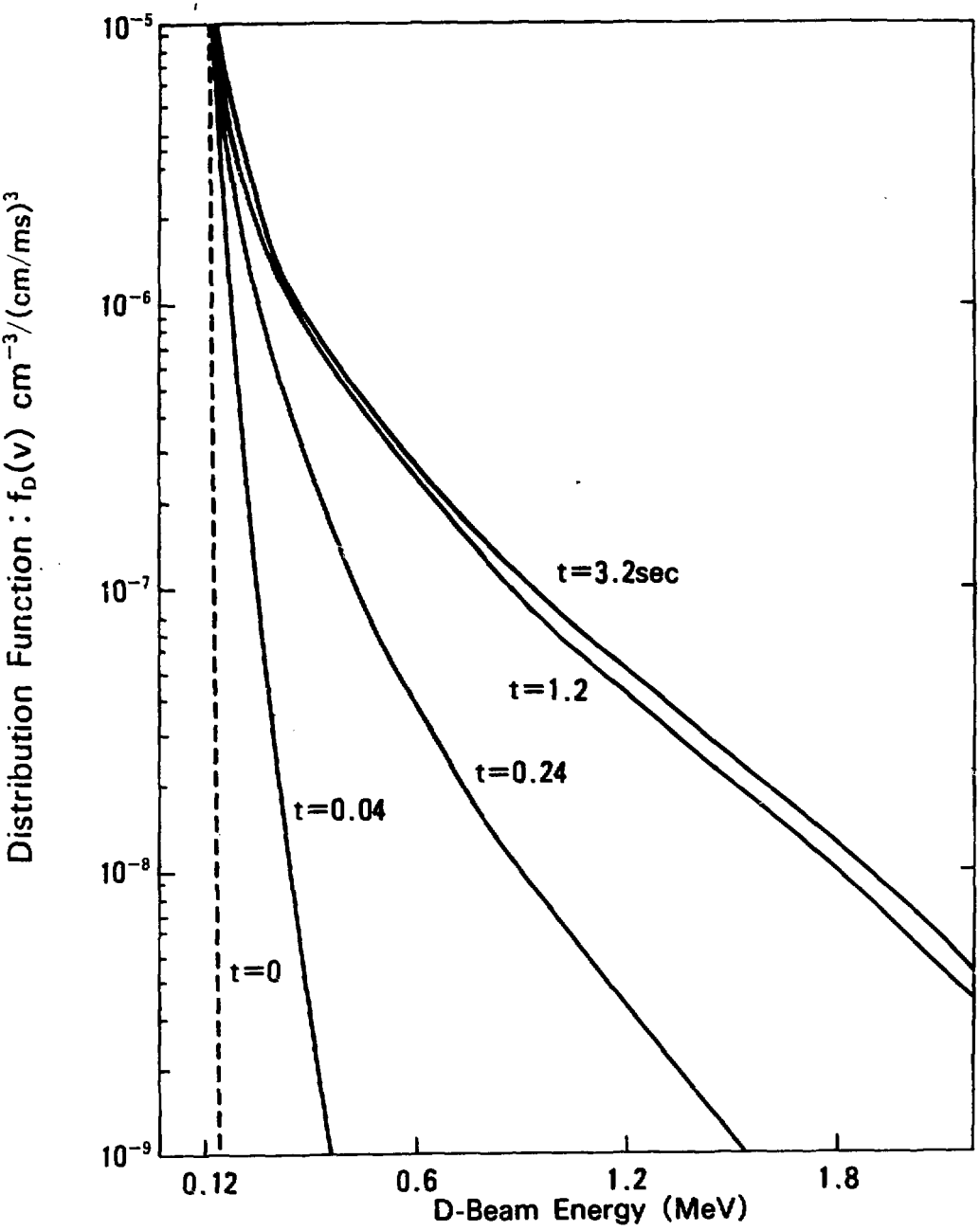
Distribution Function : $f_D(v)$ $cm^{-3}/(cm/ms)^3$
10^{-5}
10^{-6}
10^{-7}
10^{-8}
10^{-9}
t=3.2sec
t=1.2
t=0.24
t=0.04
t=0
0.12
0.6
1.2
1.8
D-Beam Energy (MeV)

Fig. 3

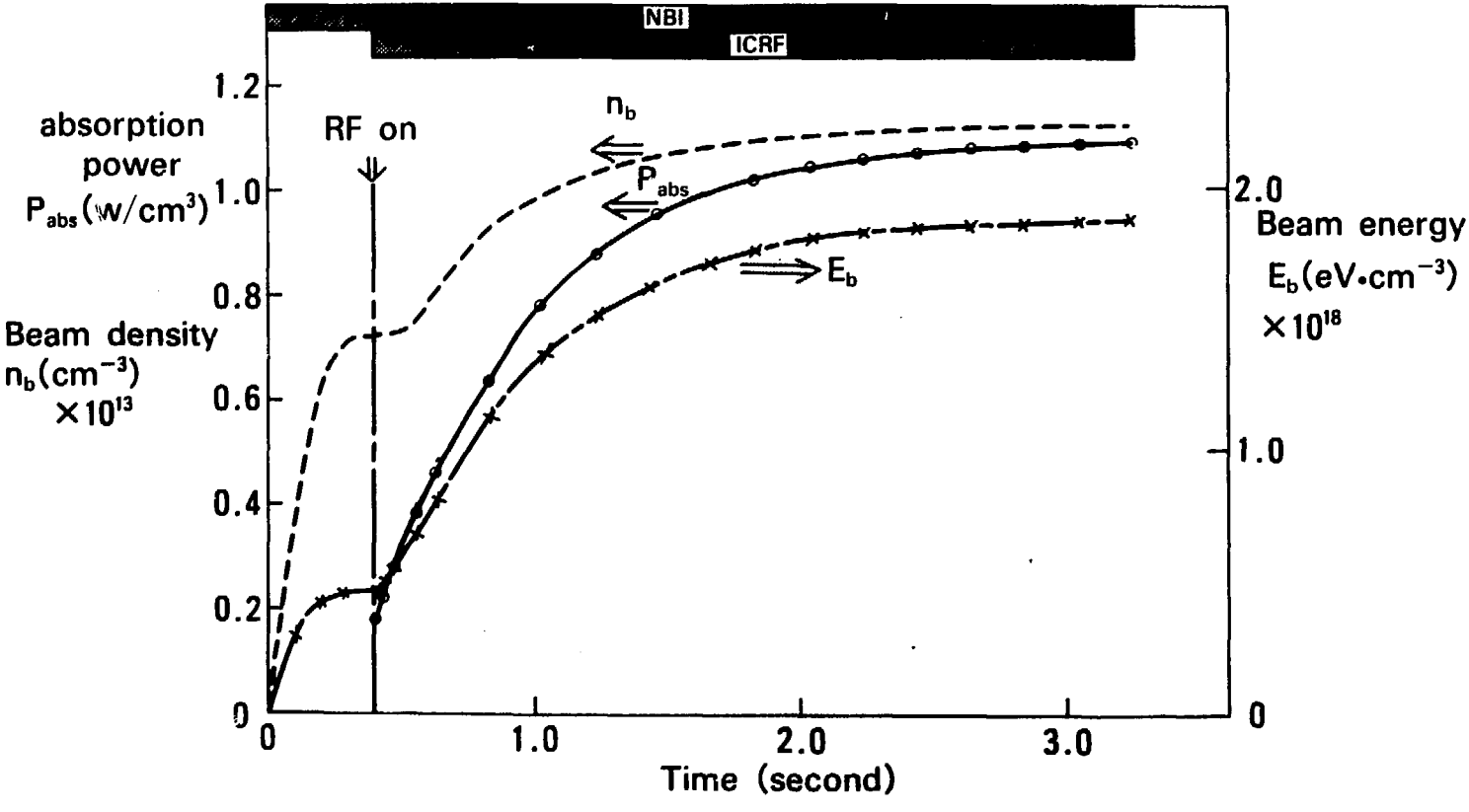
NBI
ICRF
RF on
n_b
P_{abs}
E_b
absorption power
P_{abs}(w/cm^3)
Beam density
n_b(cm^{-3})
×10^{13}
Beam energy
E_b(eV•cm^{-3})
×10^{18}
1.2
1.0
0.8
0.6
0.4
0.2
0
2.0
1.0
0
0
1.0
2.0
3.0
Time (second)

Fig. 4

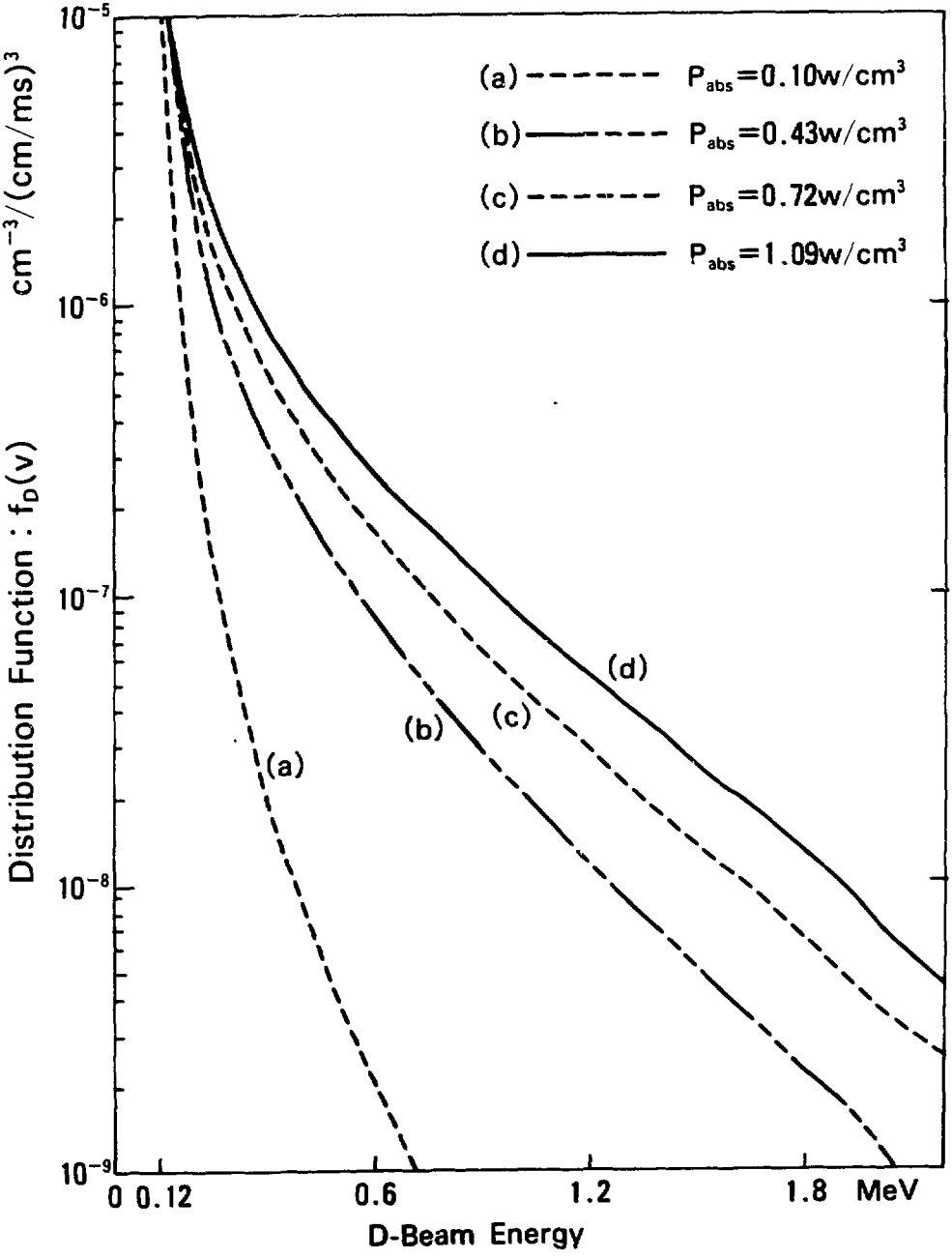
(a) P_{abs}=0.10w/cm^3
(b) P_{abs}=0.43w/cm^3
(c) P_{abs}=0.72w/cm^3
(d) P_{abs}=1.09w/cm^3
Distribution Function : $f_D(v)$ cm^{-3}/(cm/ms)^3
10^{-5}
10^{-6}
10^{-7}
10^{-8}
10^{-9}
(a)
(b)
(c)
(d)
0 0.12
0.6
1.2
1.8 MeV
D-Beam Energy

Fig. 5

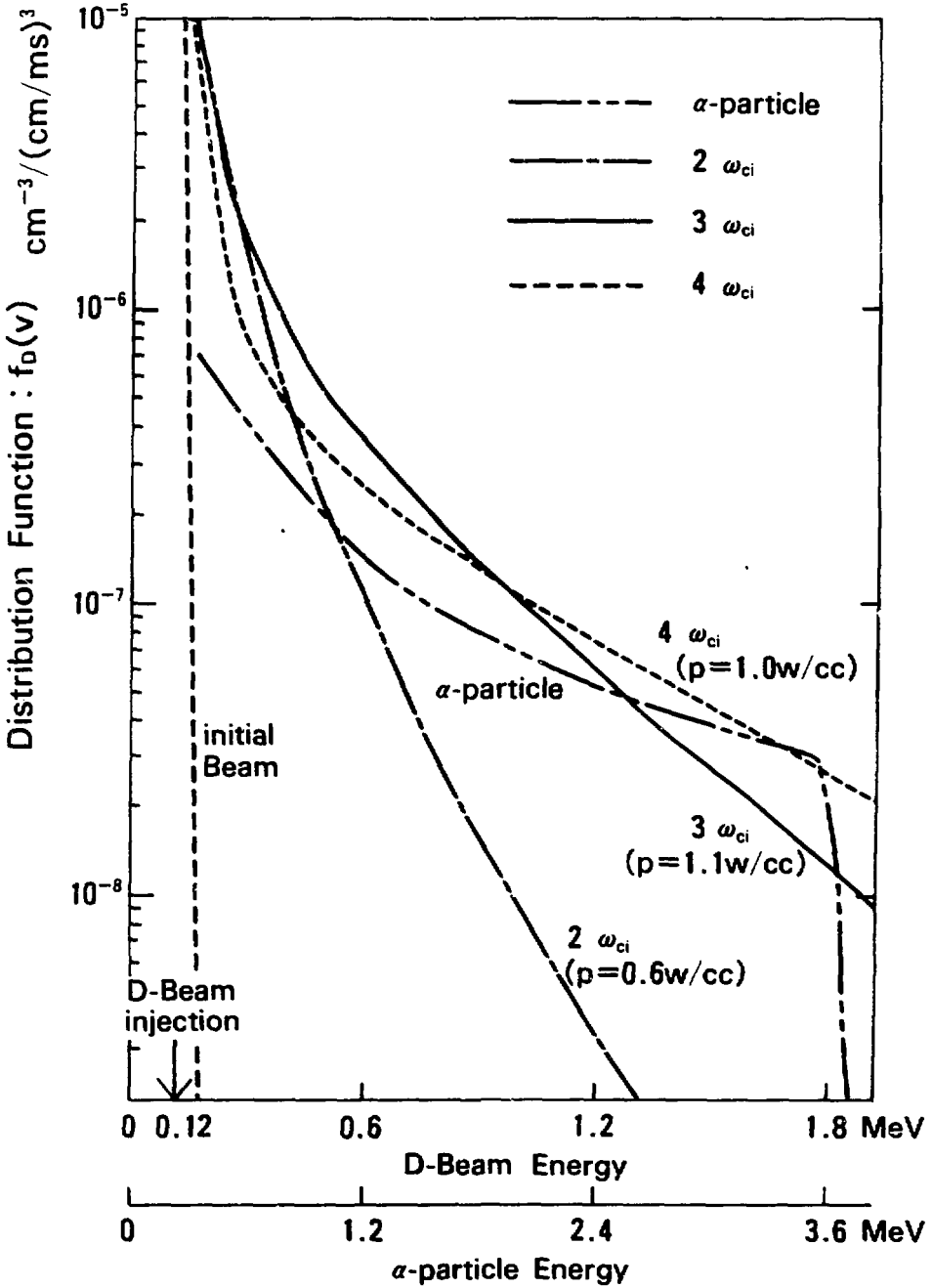
Distribution Function : $f_D(v)$ $cm^{-3}/(cm/ms)^3$
10^{-5}
10^{-6}
10^{-7}
10^{-8}
α-particle
2 ω_{ci}
3 ω_{ci}
4 ω_{ci}
4 ω_{ci} (p=1.0w/cc)
α-particle
initial Beam
3 ω_{ci} (p=1.1w/cc)
2 ω_{ci} (p=0.6w/cc)
D-Beam injection
0 0.12 0.6 1.2 1.8 MeV
D-Beam Energy
0 1.2 2.4 3.6 MeV
α-particle Energy

Fig. 6

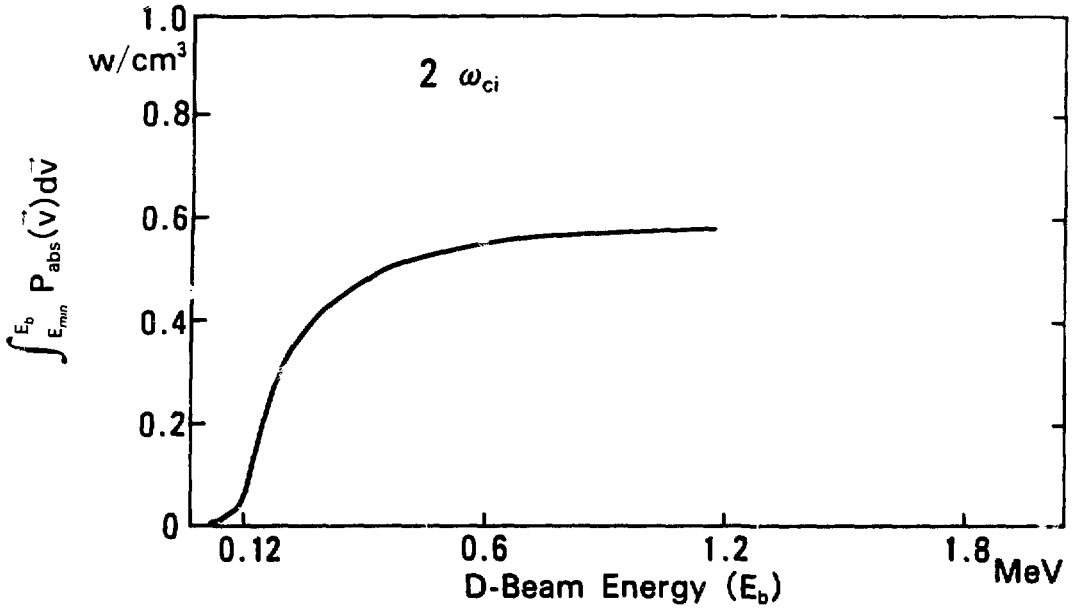
1.0
w/cm³
2 ω_ci
0.8
0.6
0.4
0.2
0
∫ E_min to E_b P_abs(v)dv
0.12
0.6
1.2
1.8
MeV
D-Beam Energy (E_b)

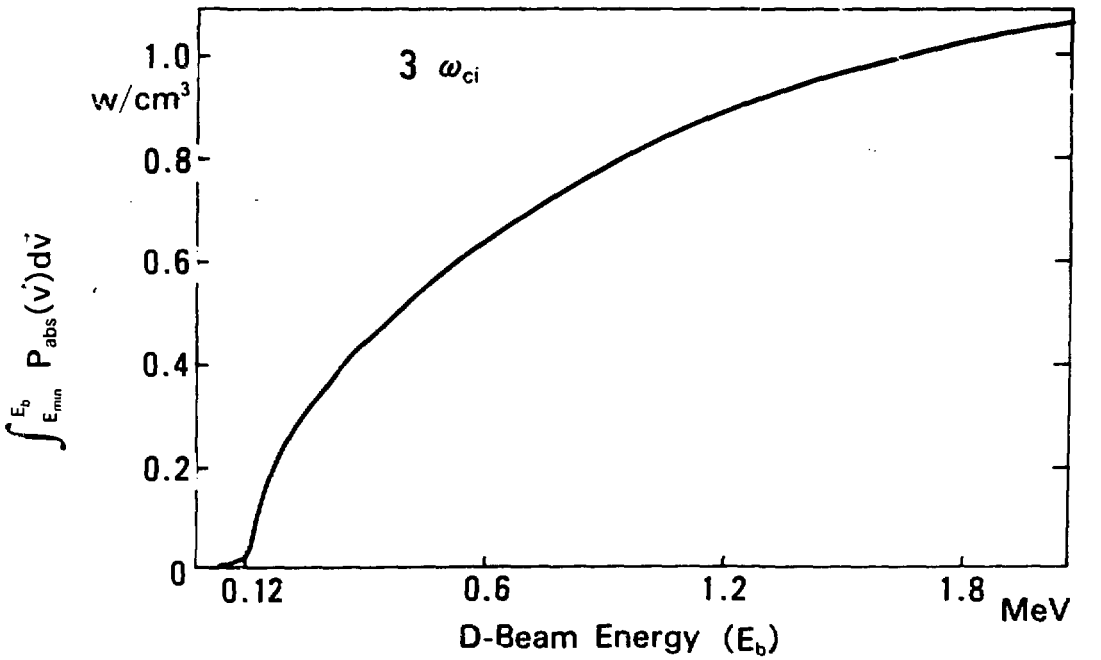
1.0
w/cm³
3 ω_ci
0.8
0.6
0.4
0.2
0
∫ E_min to E_b P_abs(v)dv
0.12
0.6
1.2
1.8
MeV
D-Beam Energy (E_b)

Fig. 7

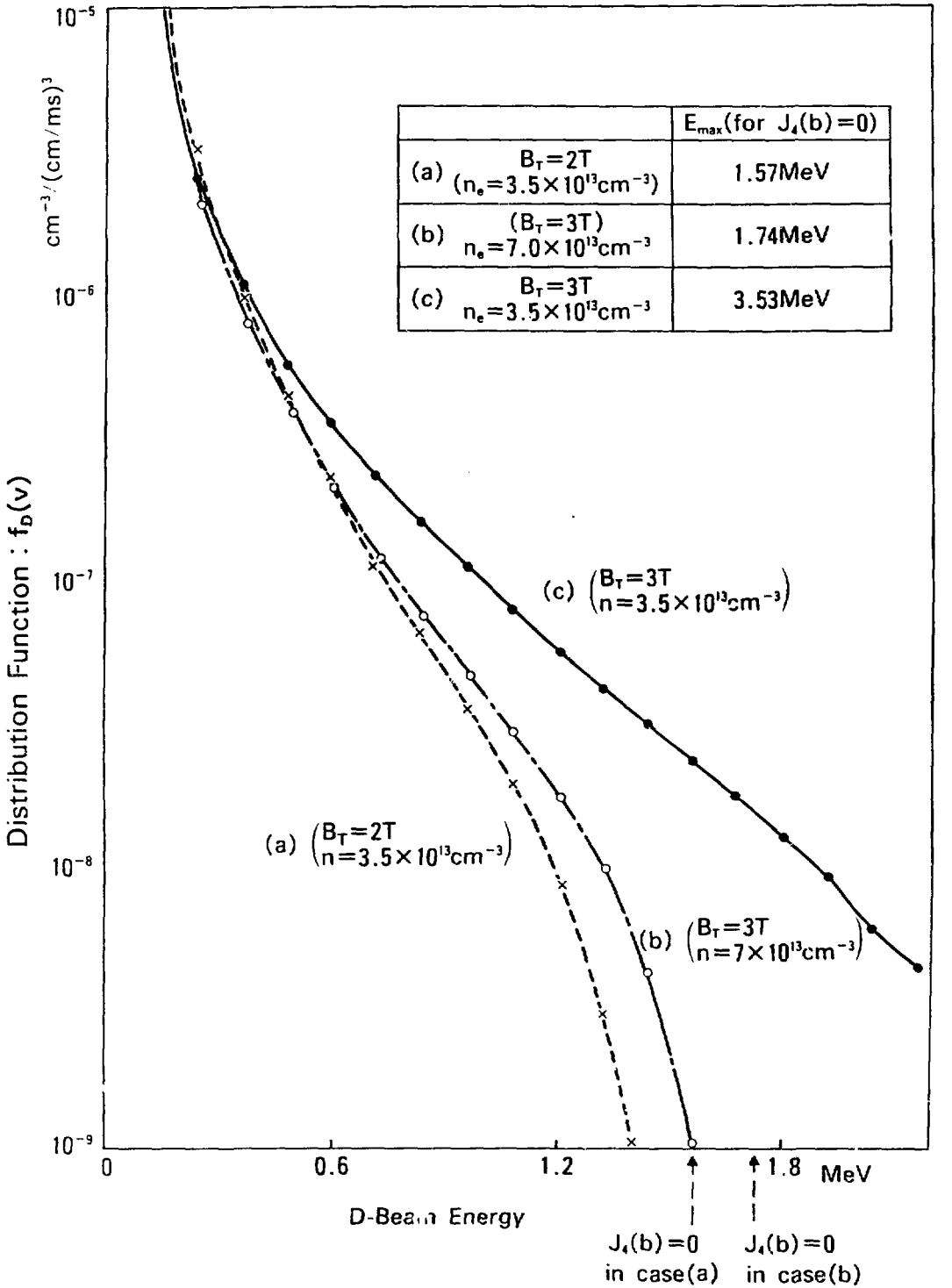
Distribution Function : $f_D(v)$
$cm^{-3}/(cm/ms)^3$
10^{-5}
10^{-6}
10^{-7}
10^{-8}
10^{-9}
0
0.6
1.2
1.8 MeV
D-Beam Energy
E_{max}(for $J_4(b)=0$)
(a) $B_T=2T$ ($n_e=3.5\times10^{13}cm^{-3}$) 1.57MeV
(b) ($B_T=3T$) $n_e=7.0\times10^{13}cm^{-3}$ 1.74MeV
(c) $B_T=3T$ $n_e=3.5\times10^{13}cm^{-3}$ 3.53MeV
(c) ($B_T=3T$ $n=3.5\times10^{13}cm^{-3}$)
(a) ($B_T=2T$ $n=3.5\times10^{13}cm^{-3}$)
(b) ($B_T=3T$ $n=7\times10^{13}cm^{-3}$)
$J_4(b)=0$ in case(a)
$J_4(b)=0$ in case(b)

Fig. 8

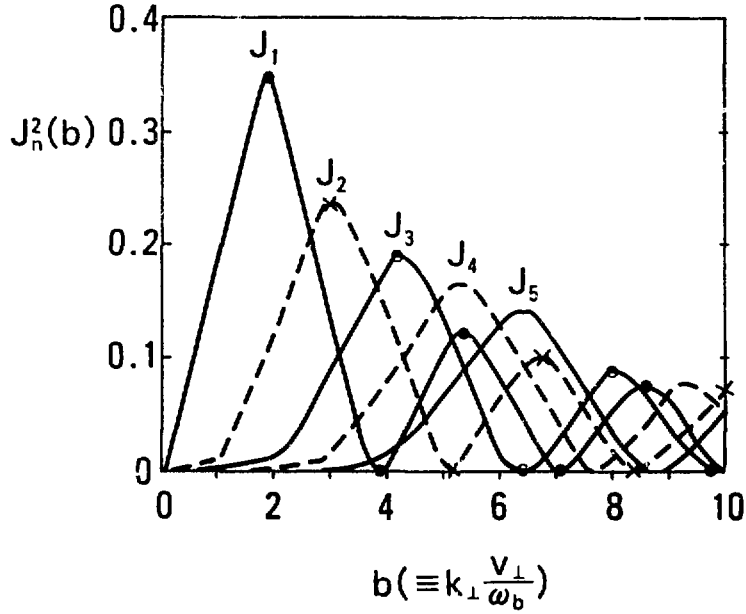
0.4
0.3
0.2
0.1
0
$J_n^2(b)$
J_1
J_2
J_3
J_4
J_5
0
2
4
6
8
10
$b(\equiv k_\perp \frac{v_\perp}{\omega_b})$

Fig. 9(a)

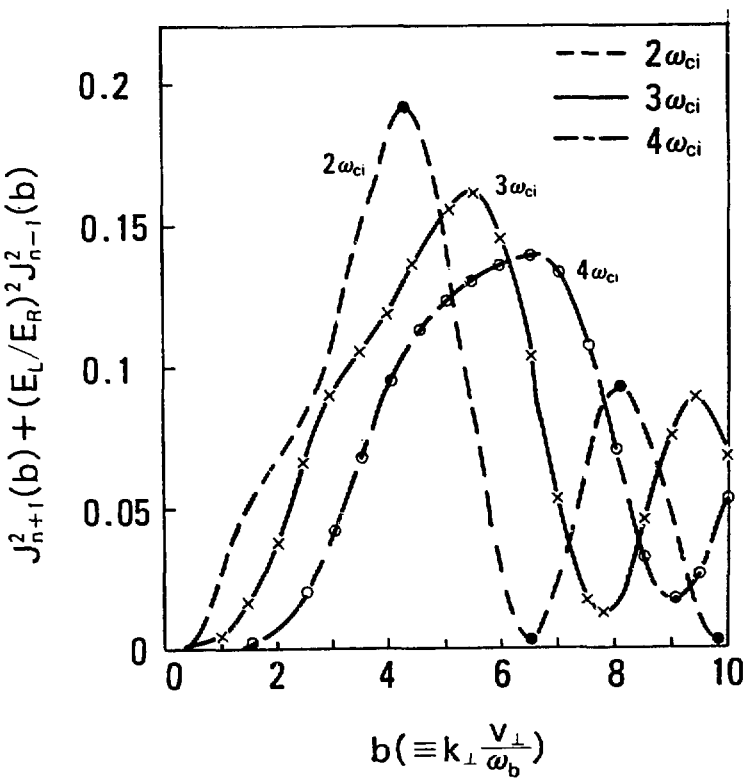
$2\omega_{ci}$
$3\omega_{ci}$
$4\omega_{ci}$
0.2
0.15
0.1
0.05
0
$J_{n+1}^2(b) + (E_L/E_R)^2 J_{n-1}^2(b)$
$2\omega_{ci}$
$3\omega_{ci}$
$4\omega_{ci}$
0
2
4
6
8
10
$b(\equiv k_\perp \frac{v_\perp}{\omega_b})$

Fig. 9(b)